

Notably, this paper for the first time, to the best of our knowledge, unifies the ViT and the contrastive learning for the image clustering task. To make this unification possible and practical, some critical challenges should be handled. Different from CNN [2], the training recipes for ViT are often sensitive, especially in the self-supervised scenarios [12], which involve the choice of hyper-parameters, the number of encoder blocks, and so forth. As a consequence, the training of ViT usually needs a large dataset, and the instability issue is often encountered [13], [15], [16]. Recently, some studies suggest that this issue may arise from the patch projection layer in the standard ViT. Regarding this, Chen et al. [12] alleviated the instability issue by freezing the patchify stem instead of using the random initialization patch projection layer. Xiao et al. [16] replaced the origin patchify stem with a convolutional stem, which is implemented by a small number of stacked stride-2 3×3 convolutions in the patch projection layer. In this work, we observe that the use of multiple stacked small convolutions instead of a big convolution in the patch projection layer, which to some extent resembles the typical design of CNNs [2], [17], can significantly benefit the contrastive image clustering with Transformer, even for some relative small datasets.

Specifically, we propose a novel deep clustering approach termed **Vision Transformer for Contrastive Clustering (VTCC)** (as illustrated in Fig. 1). To remedy the potential instability, a convolutional stem layer with multiple stacked small-size convolutions is incorporated to split each augmented sample image into a sequence of patches. With two random augmentations performed on each image to obtain two augmented samples, we feed the sequences of patch vectors of the augmented samples to the backbone, which encompasses two weight-sharing views in a standard Transformer encoder architecture. With the representations of the augmented samples learned by the self-attention mechanism, the contrastive learning is enforced via an instance projector and a cluster projector, which explore the instance contrastiveness and the global clustering structure, respectively. Note that the Transformer backbone with convolutional stem and the two contrastive projectors in VTCC are jointly trained in an end-to-end manner. Extensive experiments are conducted on eight challenging image datasets, which confirm the benefits brought in by the Transformer, and demonstrate the stability (during the training-from-scratch) and the superior clustering performance of VTCC in comparison with the state-of-the-art.

The main contributions of this work are summarized below.

- This paper makes the first attempt to effectively bridge the gap between the Transformer and the contrastive learning for the deep image clustering task, with the global dependencies, the instance contrastiveness, and the clustering structure learning jointly modeled.
- This paper incorporates a convolutional stem with multiple stacked small convolutions in the patch projection layer, which enhances the stability during the ViT training from scratch for image clustering.
- This paper presents an end-to-end deep clustering approach termed VTCC with ViT and contrastive learning jointly modeled. Experimental results on eight real-world

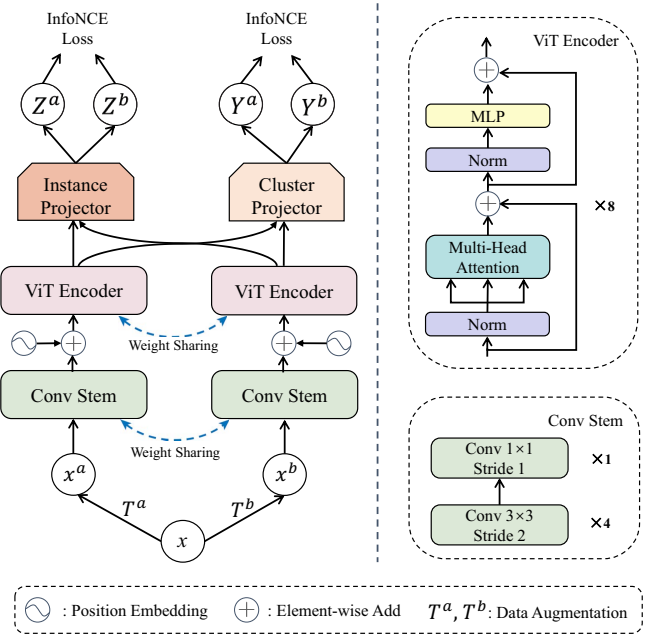


Fig. 1. **Vision Transformer for Contrastive Clustering (VTCC).**

image datasets demonstrate the promising capability of Transformer for the clustering of complex images and the advantages of VTCC over the state-of-the-art deep clustering approaches.

The remainder of the paper is organized as follows. The proposed VTCC approach is described in Section II. The experimental results are provided in Section III, followed by the conclusion in Section IV.

II. PROPOSED FRAMEWORK

In this section, we describe the details of our VTCC approach. First, an overview of the network architecture is given in Section II-A. Then the ViT backbone is presented in Section II-B. Finally, the overall loss function of VTCC is provided in Section II-C.

A. Network Architecture

The architecture of VTCC is illustrated in Fig. 1, which consists of three main components, namely, the ViT backbone with two weight-sharing views to extract feature representations for augmented samples, the instance-level contrastive learning module to maximize the similarity of positive pairs, and the global clustering structure learning module that obtains the soft label prediction for image clustering.

Specifically, for each image in a mini-batch of N images, two data augmentations T^a and T^b are randomly selected with a certain probability so as to obtain 2 augmented samples for this image, thus obtaining $2 \cdot N$ augmented samples for this mini-batch. Then each of the augmented samples is split into a sequence of patches by the convolutional stem with multiple stacked small convolutions in the patch projection layer [16]. With each sample split into a sequence of patches

and embedded by linear projection, a standard Transformer encoder is utilized for learning the feature representations, which are then fed to two projectors, i.e., the instance projector and the cluster projector, for instance-level contrastive learning and global clustering structure learning, respectively. The overall network is trained by two contrastive loss functions in an end-to-end manner, through which the clustering result can therefore be learned. Additionally, the pseudo-code of VTCC is presented in Algorithm 1.

Algorithm 1: VTCC: A PyTorch-like Pseudo Code

```

#  $f(\cdot)$  : Vision Transformer
#  $g_I(\cdot)$  : Instance projector
#  $g_C(\cdot)$  : Cluster projector
#  $\text{InfoNCE}(\cdot, \cdot)$  : InfoNCE loss
#  $\text{InsLoss}(\cdot, \cdot)$  : Instance-level contrastive loss
#  $\text{CluLoss}(\cdot, \cdot)$  : Global clustering contrastive loss
#  $T^a, T^b$  : Augmentations selected from family  $T$ 
for x in loader: # Load a mini-batch  $x$  with  $N$  samples
    # Obtain augmented views of  $x$ 
     $x^a, x^b = T^a(x), T^b(x)$ 
    # Extract feature representations
     $h^a, h^b = f(x^a), f(x^b)$ 
    # Map representations to subspace via  $g_I$ 
     $Z^a, Z^b = g_I(h^a), g_I(h^b)$ 
    # Map representations to subspace via  $g_C$ 
     $Y^a, Y^b = g_C(h^a), g_C(h^b)$ 

    # Loss calculation
     $\text{loss} = \text{InsLoss}(Z^a, Z^b) + \text{CluLoss}(Y^a, Y^b)$ 
     $\text{loss.backward}()$ 

     $\text{update}(f)$  # Optimize the parameters of  $f$ 

def  $\text{InsLoss}(Z^a, Z^b)$ :
    return  $(\text{InfoNCE}(Z^a) + \text{InfoNCE}(Z^b))/2$ 
def  $\text{CluLoss}(Y^a, Y^b)$ :
    return  $(\text{InfoNCE}(Y^a) + \text{InfoNCE}(Y^b))/2$ 

```

B. Backbone with Vision Transformer

Unlike the CNNs which are performed on the images directly, the Transformer encoder requires a sequence of vectors (or patches) as input. In VTCC, we utilize a convolutional stem with multiple stacked small-size convolutions to split each augmented sample into a sequence of patches, which are fed into a ViT [1] backbone. In the following, we describe the convolutional stem and the Transformer encoder in Sections II-B1 and II-B2, respectively.

1) *Convolutional Stem*: To convert a 2D image to a 1D sequence of feature embedding, a conventional strategy adopted in ViT is to apply the $p \times p$ convolution operation with a stride p to the input image (typically with $p = 16$), which is referred to as *the patchify stem*. Thus, it can directly capture a lot of non-overlapping patches with the $p \times p$ size, and then flatten these patches to form the input sequence of vectors for the Transformer encoder. However, on the one hand, this type of

convolution operation with a large convolution kernel and a large stride runs counter to the classical convolution setting in canonical neural networks [2] which usually adopt some small-size (e.g., 3×3) convolution kernels. On the other hand, the in-patch structure information often focus on relatively small receptive field, which overlooks the rich information of local associations (e.g., the spatial relationship between patches) and to some extent makes the patchify stem not sufficient with the simple linear projections.

Regarding this issue, Xiao et al. [16] proposed a convolutional stem which replaces the patchify stem in the original ViT model by a small number of stacked stride-2 3×3 convolutions. We empirically show that using the convolutional stem on the ViT patch embedding layer is particularly beneficial for our image clustering task (as evaluated in Section III-D). Specifically, to obtain the 1D image sequence, we first use four blocks in the convolutional stem, where each block includes a standard convolution operation with a stride-2 3×3 convolution kernel, followed by the batch normalization and a ReLU activation function (as shown in Fig. 1). Since the Transformer encoder requires the 1D image sequence as input, we use a single 1×1 convolution to match the input dimension of the Transformer encoder. In practice, compared with the large convolution, using multiple small convolutions can capture the fine-grained local features which are more conducive to the representation learning process and further contribute to better stability and clustering performance.

2) *Transformer Encoder*: In the literature, ViT models with various scales have been developed. In this paper, we adopt the ViT-Small [18] as the backbone which provides effective representation learning capability while maintaining high efficiency. Specifically, based on the input sequence of patches embedding, each encoder layer is built upon a standard Transformer architecture that consists of a multi-head self-attention and a MLP block. In addition, a layer-norm operation is adopted *before* each block, and the residual connection is incorporated *after* each block. Here, the Transformer encoder applies the self-attention layers to model global relations between input embeddings, which has an advantage over the CNNs whose receptive field of convolutional kernels are limited locally. However, the Transformer architecture is permutation-invariant theoretically, which may neglect the rich information of relative positions. Therefore, we also incorporate the position encodings [3] to the input sequence of each self-attention layer.

C. Loss Function

To simultaneously perform the instance-level and cluster-level self-supervision, two independent projectors are utilized to map the feature representations extracted by the backbone to different subspaces (i.e., the instance subspace and the cluster subspace). By means of these two projectors, the instance-level contrastive learning and the cluster-level contrastive learning are respectively enforced.

1) *Instance-level Contrastive Learning*: The purpose of the instance-level contrastive learning is to maximize the similarity between two different augmented samples of the same input

image by pulling closer the distance between a positive pair while pushing away the representations of the negative pairs in the instance subspace. Let x_i^a and x_i^b denote the two augmented samples for the input image x_i , and h_i^a and h_i^b denote the feature representations of x_i^a and x_i^b , respectively, extracted by the ViT encoder. Since directly using the feature representations h_i^a and h_i^b for similarity calculation may lead to the loss of information [6], we utilize an instance projector with a three-layer MLP, which is denoted as g_I and maps the representations h_i^a and h_i^b to a low-dimensional subspace, leading to $Z_i^a = g_I(h_i^a)$ and $Z_i^b = g_I(h_i^b)$, respectively. Then, the cosine similarity is used to measure the pair-wise similarity, that is

$$s(\alpha, \beta) = \frac{\alpha^\top \beta}{\|\alpha\| \cdot \|\beta\|}, \quad (1)$$

where α and β are two feature vectors with the same dimension.

Let I denote the instance-level representations set, which contains all the instance-level augmented representations in a mini-batch of N images, that is, $I = \{Z_1^a, \dots, Z_N^a, Z_1^b, \dots, Z_N^b\}$, where Z_i^a (or Z_i^b) is the instance-level representation of sample x_i^a (or x_i^b , respectively). Thus we can obtain $2 \cdot N - 1$ sample pairs for each augmented sample (say, Z^a), that is, $\{Z_i^a, Z_j^k\}$ with $Z_i^a \neq Z_j^k$, $k \in \{a, b\}$ and $j \in [1, N]$. Among these pairs, only the pair $\{Z_i^a, Z_i^b\}$ is the positive pair for Z_i^a , while the rest are negative pairs. Then the InfoNCE loss [11] for calculating the instance-level contrastiveness is defined as

$$l_i^a = -\log \frac{\exp(s(Z_i^a, Z^+)/\tau_I)}{\sum_{Z^- \in I} \exp(s(Z_i^a, Z^-)/\tau_I)} \quad (2)$$

where τ_I is the instance-level temperature parameter, Z^+ and Z^- are the positive and negative samples of the current sample, respectively. Thus for the image x_i , the instance-level loss is calculated as

$$l_i = l_i^a + l_i^b, \quad (3)$$

where l_i^a is the instance-level contrastive loss of x_i in the first view (and l_i^b for the second view). Finally, the instance-level contrastive loss for a mini-batch of N input images is defined as [6]

$$L_{ins} = \frac{\sum_{i=1}^N l_i}{2N}. \quad (4)$$

2) *Global Clustering Structure Learning*: Besides the instance-level contrastive loss, we proceed to define the cluster-level contrastive loss for global clustering structure learning. It aims to maximize the similarity of the positive cluster pairs while minimizing the similarity of the negative cluster pairs. A cluster projector g_C with a three-layer MLP and an extra softmax layer is incorporated to map the feature representations to the low-dimensional subspace, leading to $Y_i^a = g_C(h_i^a)$ and $Y_i^b = g_C(h_i^b)$. For a mini-batch of N input images, we can obtain the cluster distribution probability matrices $Y^a \in \mathbb{R}^{N \times K}$ and $Y^b \in \mathbb{R}^{N \times K}$ for the two augmented views by stacking the learned representations of the N samples, where K is the number of clusters and the

i -th column (i.e., the representation of i -th cluster, denoted as \hat{Y}_i^k with $k \in \{a, b\}$) of these two matrices indicates the probability of allocating each sample to the i -th cluster.

Let C denote the cluster-level representation set which contains the representations of all clusters (in the two augmented views), that is, $C = \{\hat{Y}_1^a, \dots, \hat{Y}_K^a, \hat{Y}_1^b, \dots, \hat{Y}_K^b\}$. We take the cluster representations from C to construct cluster pairs. Formally, for each cluster, say, \hat{Y}_i^a , we can obtain $2 \cdot K - 1$ cluster pairs, that is, $\{\hat{Y}_i^a, \hat{Y}_j^k\}$ with $\hat{Y}_j^k \neq \hat{Y}_i^a$, $k \in \{a, b\}$ and $j \in [1, K]$. For the cluster \hat{Y}_i^a , only the pair $\{\hat{Y}_i^a, \hat{Y}_i^b\}$ is a positive cluster pair, while the rest are negative pairs. By using the cosine similarity to measure the similarity between the cluster representations, the cluster-level contrastive loss for \hat{Y}_i^a is defined as

$$\hat{l}_i^a = -\log \frac{\exp(s(\hat{Y}_i^a, Y^+)/\tau_C)}{\sum_{Y^- \in C} \exp(s(\hat{Y}_i^a, Y^-)/\tau_C)} \quad (5)$$

where τ_C is the cluster-level temperature parameter, Y^+ and Y^- are the positive and negative clusters of the current cluster, respectively. The contrastive loss for the both augmented views of the i -th cluster is defined as

$$\hat{l}_i = \hat{l}_i^a + \hat{l}_i^b, \quad (6)$$

where \hat{l}_i^a is the cluster-level contrastive loss of the i -th cluster in the first view (and \hat{l}_i^b in the second view). Then the cluster-level contrastive loss for the K clusters is defined as [14]

$$L_{clu} = \frac{1}{2K} \sum_{i=1}^K \hat{l}_i - Entropy(p(Y^a)) - Entropy(p(Y^b)). \quad (7)$$

To avoid the trivial solution that assigns most samples to a single cluster, the entropy term is incorporated into the loss function, which is defined as

$$Entropy(p(Y^k)) = -\sum_{i=1}^K [p(\hat{Y}_i^k) \log p(\hat{Y}_i^k)], \quad (8)$$

$$p(\hat{Y}_i^k) = \frac{\sum_{j=1}^N y_{ji}^k}{\|\hat{Y}_i^k\|_1}, \text{ for } k \in \{a, b\}, \quad (9)$$

where y_{ji}^a (or y_{ji}^b) denotes the entry in the j -th row and i -th column of the representation matrix Y^a (or Y^b , respectively).

3) *Overall Loss Function*: By minimizing the losses (4) and (7), the network can be trained by maximizing the similarity between the representations of the positive pairs, while minimizing the similarity between the representations of the negative pairs, at the instance-level and the cluster-level, respectively.

In VTCC, we jointly optimize the losses L_{ins} and L_{clu} to enforce the instance-level and cluster-level contrastive learning and obtain the clustering result. The overall loss function is defined as

$$L_{total} = L_{ins} + L_{clu}. \quad (10)$$

III. EXPERIMENTS

In this section, we conduct experiments on eight real-world image datasets to evaluate the proposed VTCC approach against a variety of non-deep and deep clustering approaches.

TABLE I
THE IMAGE DATASETS USED IN OUR EXPERIMENTS.

Dataset	#Samples	#Classes
RSOD [19]	976	4
UC-Merced [20]	2,100	21
SIRI-WHU [21]	2,400	12
AID [22]	10,000	30
D0 [23]	4,508	40
DTD [24]	5,640	47
Chaoyang [25]	6,160	4
CIFAR-100 [26]	60,000	20

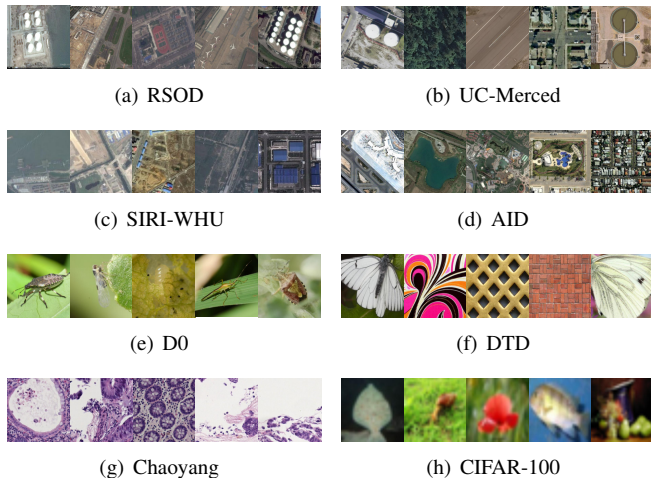


Fig. 2. Some examples of the eight real-world image datasets used for evaluation, including four remote sensing datasets [19]–[22], a crop pest dataset [23], a texture dataset [24], a medical dataset [25], and an object image dataset [26].

A. Implementation Details

In this work, we adopt the setting of data augmentations in BYOL [27] and use the Adam optimizer with an initial learning rate of 0.0003. A lightweight version of ViT, i.e., ViT-Small [18], is utilized as our backbone with a dimension size of 384 and 8 blocks of encoder layers. The input image size is set to 224×224 . We leverage a convolutional stem with four small 3×3 convolutions instead of a large 16×16 convolution, followed by 1×1 convolution. The instance projector and the cluster projector each uses a three-layer MLP, following the projector network of MoCov3 [12]. Besides, we set the output dimension of the instance projector to 128, which can preserve sufficient information for the instance-level contrastive learning. As for the cluster projector, the output dimension is set to the number of clusters, i.e., the true number of classes on each dataset. The temperature parameters τ_I and τ_C are set to 0.5 and 1.0, respectively. We train the VTCC architecture from scratch for 1,000 epochs with a batch size of 128. All experiments are conducted on a single NVIDIA RTX 3090 GPU and CUDA 11.0.

B. Datasets and Evaluation Metrics

In our experiments, eight real-world image datasets are used for evaluation, which are described as follows:

- **RSOD** [19] is a classical dataset for the remote sensing task, which consists of 976 images with 4 different classes, including aircraft, oil tank, overpass, and playground.
- **UC-Merced** [20] is a collection of 2,100 images with 21 different scenes and 100 images per category.
- **SIRI-WHU** [21] is another remote sensing image dataset, which contains a total of 2,400 images in 12 categories, where each category includes 200 images.
- **AID** [22] is a large remote sensing dataset, including 30 categories of scene images and a total of 10,000 images.
- **D0** [23] consists of 4,508 images with 40 pest classes, which were collected under real-world conditions in a variety of fields.
- **DTD** [24] is a complex texture dataset, which consists of 5,640 images with 47 different classes.
- **Chaoyang** [25] is a medical dataset with 6,160 images and 4 classes of the colon slides, collected from Chaoyang hospital.
- **CIFAR-100** [26] is a widely-used object image dataset. We use its 20 super-classes as the ground-truth.

For clarity, we summarize the statistics of the eight image dataset in Table I and illustrate some sample images of them in Fig. 2.

Following the standard evaluation protocol for the image clustering task, we adopt three widely-used evaluation metrics in the experiments, including the normalized mutual information (NMI) [28], the accuracy (ACC) [29], and the adjusted Rand index (ARI) [30]. Note that higher values of these metrics indicate better clustering results.

C. Comparisons with State-of-the-Art methods

In this section, we evaluate the performance of the proposed VTCC method against twelve baseline clustering methods, including seven traditional clustering methods and five deep clustering methods. The seven traditional clustering methods include K -means [31], Spectral Clustering (SC) [32], Agglomerative Clustering (AC) [33], Non-negative Matrix Factorization (NMF) [34], Principle Component Analysis (PCA) [35], Balanced Iterative Reducing and Clustering using Hierarchies (BIRCH) [36], Gaussian Mixture Model (GMM) [37], whereas the five deep clustering methods include Deep Embedding Clustering (DEC) [38], Improved Deep Embedding Clustering (IDEC) [39], Adaptive Self-Paced Deep Clustering with Data Augmentation (ASPC-DA) [40], Instance Discrimination and Feature Decorrelation (IDFD) [41], and Contrastive Clustering (CC) [14]. For NMF and PCA, the clustering results are obtained by conducting K -means on the dimensionally-reduced features. For the other baseline algorithms, the hyper-parameters will be set as suggested by their corresponding papers. For each test method, the number of clusters is set to the true number of classes on this dataset. The experimental results w.r.t. NMI, ACC, and ARI by different deep and non-deep clustering methods are reported in Tables II, III, and IV, respectively.

In terms of NMI, as shown in Table II, our VTCC method outperforms the baseline methods on all the eight datasets.

TABLE II
THE NMI SCORES OF DIFFERENT IMAGE CLUSTERING METHODS ON EIGHT DATASETS.

Dataset	RSOD	UC-Merced	SIRI-WHU	AID	D0	DTD	Chaoyang	CIFAR-100
<i>K</i> -means [31]	0.162	0.204	0.145	0.209	0.299	0.119	0.024	0.083
SC [32]	0.146	0.211	0.161	0.189	0.305	0.118	0.022	0.090
AC [33]	0.168	0.214	0.166	0.204	0.319	0.125	0.026	0.098
NMF [34]	0.176	0.202	0.245	0.193	0.255	0.127	0.018	0.076
PCA [35]	0.163	0.206	0.164	0.216	0.308	0.124	0.024	0.084
BIRCH [36]	0.148	0.225	0.162	0.204	0.315	0.123	0.026	-
GMM [37]	0.160	0.198	0.160	0.205	0.289	0.120	0.024	0.084
DEC [38]	0.296	0.120	0.183	0.217	0.328	0.128	0.001	0.101
IDEC [39]	0.209	0.119	0.178	0.207	0.309	0.128	0.001	0.103
ASPC-DA [40]	0.054	0.137	0.103	0.060	0.153	0.084	0.026	-
IDFD [41]	0.391	0.572	0.540	0.696	0.663	0.410	0.309	0.428
CC [14]	0.457	0.609	0.603	0.752	0.693	0.480	0.365	0.424
VTCC (Ours)	0.611	0.658	0.693	0.794	0.753	0.487	0.373	0.432

TABLE III
THE ACC SCORES OF DIFFERENT IMAGE CLUSTERING METHODS ON EIGHT DATASETS.

Dataset	RSOD	UC-Merced	SIRI-WHU	AID	D0	DTD	Chaoyang	CIFAR-100
<i>K</i> -means [31]	0.388	0.200	0.229	0.163	0.204	0.090	0.320	0.137
SC [32]	0.425	0.183	0.210	0.123	0.195	0.091	0.312	0.136
AC [33]	0.371	0.188	0.222	0.151	0.209	0.091	0.329	0.138
NMF [34]	0.420	0.208	0.275	0.161	0.187	0.091	0.305	0.127
PCA [35]	0.388	0.198	0.227	0.173	0.220	0.090	0.320	0.139
BIRCH [36]	0.396	0.202	0.222	0.147	0.205	0.092	0.329	-
GMM [37]	0.382	0.193	0.239	0.169	0.189	0.091	0.318	0.132
DEC [38]	0.534	0.147	0.257	0.185	0.232	0.092	0.421	0.157
IDEC [39]	0.458	0.141	0.255	0.192	0.213	0.094	0.424	0.160
ASPC-DA [40]	0.464	0.073	0.183	0.079	0.107	0.067	0.325	-
IDFD [41]	0.595	0.456	0.545	0.628	0.507	0.306	0.512	0.424
CC [14]	0.538	0.480	0.604	0.622	0.511	0.358	0.575	0.426
VTCC(Ours)	0.572	0.553	0.670	0.716	0.575	0.393	0.585	0.455

TABLE IV
THE ARI SCORES OF DIFFERENT IMAGE CLUSTERING METHODS ON EIGHT DATASETS.

Dataset	RSOD	UC-Merced	SIRI-WHU	AID	D0	DTD	Chaoyang	CIFAR-100
<i>K</i> -means [31]	0.075	0.065	0.053	0.051	0.080	0.016	0.017	0.028
SC [32]	0.096	0.038	0.041	0.029	0.039	0.012	0.005	0.022
AC [33]	0.071	0.057	0.057	0.048	0.080	0.015	0.010	0.034
NMF [34]	0.052	0.089	0.118	0.056	0.068	0.017	0.002	0.023
PCA [35]	0.075	0.064	0.063	0.054	0.088	0.015	0.017	0.029
BIRCH [36]	0.068	0.066	0.049	0.046	0.080	0.016	0.010	-
GMM [37]	0.069	0.062	0.062	0.053	0.074	0.015	0.016	0.028
DEC [38]	0.325	0.053	0.083	0.075	0.105	0.017	0.006	0.039
IDEC [39]	0.144	0.042	0.079	0.073	0.093	0.017	-	0.042
ASPC-DA [40]	0.005	0.002	0.035	0.014	0.021	0.005	0.005	-
IDFD [41]	0.362	0.354	0.389	0.547	0.439	0.174	0.259	0.276
CC [14]	0.371	0.356	0.450	0.550	0.423	0.205	0.343	0.267
VTCC(Ours)	0.482	0.453	0.554	0.622	0.509	0.233	0.351	0.281

Especially, on the RSOD dataset, VTCC achieves an NMI of 0.611, while the second best method (i.e., the CC method) only obtains an NMI of 0.457, where a relative gain of 33.7% is observed. It is worth noting that the RSOD dataset is a small dataset with only 976 samples and that our VTCC model is trained from scratch. As for the other bigger datasets, our VTCC method also exhibits better or significantly better clustering performance than the baseline methods. In terms of ACC and ARI, as shown in Tables III and IV, similar advantages of VTCC can be seen in comparison with the

other deep and non-deep clustering methods. The experimental results demonstrate the superiority of our VTCC method which jointly leverages Transformer encoder and contrastive learning for the clustering of complex images.

D. Ablation Study

In this section, we experimentally analyze the influence of different components in VTCC, including the convolutional stem, the ViT architecture, and the two contrastive projectors, on the RSOD and Chaoyang datasets.

TABLE V
THE INFLUENCE OF THE CONVOLUTIONAL STEM.

Dataset	Split method	NMI	ACC	ARI
RSOD	Patchify Stem	0.570	0.565	0.461
	Convolutional Stem	0.611	0.572	0.482
Chaoyang	Patchify Stem	0.365	0.573	0.336
	Convolutional Stem	0.373	0.585	0.351

TABLE VI
THE INFLUENCE OF ViT ARCHITECTURE.

Dataset	Model	Dimension	#Blocks	#Heads	NMI	ACC	ARI
RSOD	ViT-Tiny	192	4	12	0.557	0.563	0.454
	ViT-Small	384	8	12	0.611	0.572	0.482
	ViT-Base	768	12	12	0.480	0.554	0.393
Chaoyang	ViT-Tiny	192	4	12	0.340	0.580	0.328
	ViT-Small	384	8	12	0.373	0.585	0.351
	ViT-Base	768	12	12	0.362	0.571	0.332

TABLE VII
THE INFLUENCE OF TWO CONTRASTIVE PROJECTORS.

Dataset	Contrastive projectors	NMI	ACC	ARI
RSOD	Instance projector only + K -means	0.465	0.628	0.362
	Cluster projector only	0.529	0.618	0.425
	Instance projector + Cluster projector	0.611	0.572	0.482
Chaoyang	Instance projector only + K -means	0.343	0.478	0.240
	Cluster projector only	0.310	0.546	0.279
	Instance projector + Cluster projector	0.373	0.585	0.351

1) *Influence of Convolutional Stem*: This section conducts experiments to evaluate the influence of the convolutional stem, which is described in Section II-B1. As shown in Table V, using convolutional stem leads to an NMI score 0.611 on the RSOD dataset and 0.373 on the Chaoyang dataset, both of which are better than that of using the original patchify stem in ViT. Similar advantages in terms of ACC and ARI can also be observed, which confirm that the use of the convolutional stem is beneficial to the clustering performance of VTCC.

2) *Influence of Vision Transformer Architecture*: To evaluate the influence of the ViT architecture, we compare the performances of VTCC with different scales of Transformer encoder architectures, including ViT-Tiny [18], ViT-Small [18], and ViT-Base [18], and report the clustering results in Table VI. As shown in Table VI, on the small dataset of RSOD, ViT-Small and ViT-Tiny outperform ViT-Base, probably due to the fact that ViT-Base is the largest model (among the three) and may lead to over-fitting on the small dataset. Empirically, the ViT-Small is a suitable choice with sufficient representation learning capability while maintaining high efficiency.

3) *Influence of Contrastive Projectors*: This section conducts experiments to evaluate the influence of the two contrastive projectors in VTCC. When testing the performance of the instance projector, the cluster projector is removed and the K -means clustering is performed on the representation learned by the instance projector. As shown in Table VII, on the RSOD dataset, only using the instance projector leads to an

NMI of 0.465, whereas only using the cluster projector leads to an NMI of 0.529, both of which are lower than the NMI of jointly using two projectors, that is, 0.611. Although only using the instance projector can lead to a better ACC score than using both projectors, yet using both projectors yields the best performance in terms of the other two metrics on the RSOD dataset, and in terms of all the three metrics on the Chaoyang dataset.

E. t -SNE Visualization

Our VTCC method is capable of learning discriminative features by jointly exploiting the Transformer and the contrastive learning. In Fig. 3, we use the t -SNE [42] visualization to show the changes of the representation quality with varying number of epochs. As shown in Fig. 3, the quality of the feature representations learned by VTCC improves as the number of the training epochs goes from 0 to 500, where clear separation between clusters can be observed.

IV. CONCLUSION

This paper presents a novel deep clustering approach termed VTCC, which for the first time unifies the Transformer and the contrastive learning for the image clustering task. In particular, we utilize a ViT encoder architecture as the backbone to extract the feature representations of two augmented views, where a convolutional stem is used to split each augmented sample into a sequence of patches for the Transformer encoder. Two contrastive projectors are incorporated to simultaneously enforce the instance-level contrastive learning and the cluster-level contrastive learning (for global clustering structure learning). Extensive experiments are conducted on eight real-world image datasets, which have demonstrated the superiority of VTCC over the state-of-the-art deep clustering approaches. Notably, the experimental results reveal the benefits of the joint modeling of Transformer and contrastive learning for unsupervised image clustering, especially for images with complex structures. Starting from the VTCC approach, more Transformer architectures and contrastive learning strategies can be explored for the unsupervised image clustering task as well as other unsupervised learning tasks.

REFERENCES

- [1] A. Dosovitskiy, L. Beyer, A. Kolesnikov, D. Weissenborn, X. Zhai, T. Unterthiner, M. Dehghani, M. Minderer, G. Heigold, S. Gelly, J. Uszkoreit, and N. Houlsby, "An image is worth 16x16 words: Transformers for image recognition at scale," in *Proc. of International Conference on Learning Representations (ICLR)*, 2021.
- [2] K. He, X. Zhang, S. Ren, and J. Sun, "Deep residual learning for image recognition," in *Proc. of IEEE Conference on Computer Vision and Pattern Recognition (CVPR)*, 2016.
- [3] A. Vaswani, N. Shazeer, N. Parmar, J. Uszkoreit, L. Jones, A. N. Gomez, L. Kaiser, and I. Polosukhin, "Attention is all you need," in *Advanced in Neural Information Processing Systems (NeurIPS)*, 2017.
- [4] N. Carion, F. Massa, G. Synnaeve, N. Usunier, A. Kirillov, and S. Zagoruyko, "End-to-end object detection with transformers," in *Proc. of European Conference on Computer Vision (ECCV)*, 2020.
- [5] R. Strudel, R. Garcia, I. Laptev, and C. Schmid, "Segformer: Transformer for semantic segmentation," in *Proc. of IEEE International Conference on Computer Vision (ICCV)*, 2021.
- [6] T. Chen, S. Kornblith, M. Norouzi, and G. Hinton, "A simple framework for contrastive learning of visual representations," in *Proc. of International Conference on Machine Learning (ICML)*, 2020.

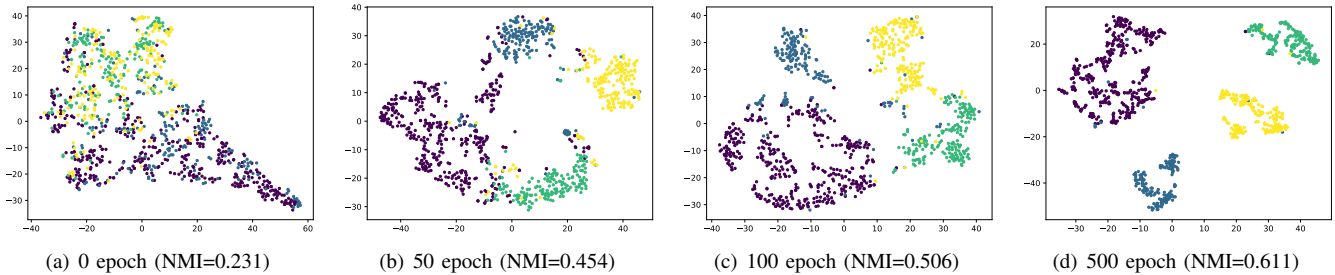


Fig. 3. The t-SNE visualization of VTCC on the RSOD dataset.

- [7] K. He, H. Fan, Y. Wu, S. Xie, and R. Girshick, "Momentum contrast for unsupervised visual representation learning," in *Proc. of IEEE Conference on Computer Vision and Pattern Recognition (CVPR)*, 2020.
- [8] X. Liu, F. Zhang, Z. Hou, L. Mian, Z. Wang, J. Zhang, and J. Tang, "Self-supervised learning: Generative or contrastive," *IEEE Transactions on Knowledge and Data Engineering*, pp. 1–1, 2021.
- [9] A. Van den Oord, N. Kalchbrenner, L. Espeholt, O. Vinyals, A. Graves *et al.*, "Conditional image generation with PixelCNN decoders," in *Advanced in Neural Information Processing Systems (NeurIPS)*, 2016.
- [10] A. Radford, L. Metz, and S. Chintala, "Unsupervised representation learning with deep convolutional generative adversarial networks," *arXiv preprint arXiv:1511.06434*, 2015.
- [11] A. v. d. Oord, Y. Li, and O. Vinyals, "Representation learning with contrastive predictive coding," *arXiv preprint arXiv:1807.03748*, 2018.
- [12] X. Chen, S. Xie, and K. He, "An empirical study of training self-supervised vision transformers," in *Proc. of IEEE International Conference on Computer Vision (ICCV)*, 2021.
- [13] M. Caron, H. Touvron, I. Misra, H. Jégou, J. Mairal, P. Bojanowski, and A. Joulin, "Emerging properties in self-supervised vision transformers," in *Proc. of IEEE International Conference on Computer Vision (ICCV)*, 2021.
- [14] Y. Li, P. Hu, Z. Liu, D. Peng, J. T. Zhou, and X. Peng, "Contrastive clustering," in *Proc. of AAAI Conference on Artificial Intelligence (AAAI)*, 2021.
- [15] Y. Liu, E. Sangineto, W. Bi, N. Sebe, B. Lepri, and M. Nadai, "Efficient training of visual transformers with small datasets," in *Advanced in Neural Information Processing Systems (NeurIPS)*, 2021.
- [16] T. Xiao, M. Singh, E. Mintun, T. Darrell, P. Dollár, and R. Girshick, "Early convolutions help transformers see better," in *Advanced in Neural Information Processing Systems (NeurIPS)*, 2021.
- [17] M. Tan and Q. Le, "Efficientnet: Rethinking model scaling for convolutional neural networks," in *Proc. of International Conference on Machine Learning (ICML)*, 2019.
- [18] H. Touvron, M. Cord, M. Douze, F. Massa, A. Sablayrolles, and H. Jégou, "Training data-efficient image transformers & distillation through attention," in *Proc. of International Conference on Machine Learning (ICML)*, 2021.
- [19] Y. Long, Y. Gong, Z. Xiao, and Q. Liu, "Accurate object localization in remote sensing images based on convolutional neural networks," *IEEE Transactions on Geoscience and Remote Sensing*, vol. 55, no. 5, pp. 2486–2498, 2017.
- [20] Y. Yang and S. Newsam, "Bag-of-visual-words and spatial extensions for land-use classification," in *Proc. of SIGSPATIAL International Conference on Advances in Geographic Information Systems*, 2010.
- [21] B. Zhao, Y. Zhong, G.-S. Xia, and L. Zhang, "Dirichlet-derived multiple topic scene classification model for high spatial resolution remote sensing imagery," *IEEE Transactions on Geoscience and Remote Sensing*, vol. 54, no. 4, pp. 2108–2123, 2015.
- [22] G.-S. Xia, J. Hu, F. Hu, B. Shi, X. Bai, Y. Zhong, L. Zhang, and X. Lu, "Aid: A benchmark data set for performance evaluation of aerial scene classification," *IEEE Transactions on Geoscience and Remote Sensing*, vol. 55, no. 7, pp. 3965–3981, 2017.
- [23] C. Xie, R. Wang, J. Zhang, P. Chen, W. Dong, R. Li, T. Chen, and H. Chen, "Multi-level learning features for automatic classification of field crop pests," *Computers and Electronics in Agriculture*, vol. 152, pp. 233–241, 2018.
- [24] M. Cimpoi, S. Maji, I. Kokkinos, S. Mohamed, and A. Vedaldi, "Describing textures in the wild," in *Proc. of IEEE Conference on Computer Vision and Pattern Recognition (CVPR)*, 2014.
- [25] C. Zhu, W. Chen, T. Peng, Y. Wang, and M. Jin, "Hard sample aware noise robust learning for histopathology image classification," *IEEE Transactions on Medical Imaging*, vol. 41, no. 4, pp. 881–894, 2021.
- [26] A. Krizhevsky, G. Hinton *et al.*, "Learning multiple layers of features from tiny images," 2009.
- [27] J.-B. Grill, F. Strub, F. Altché, C. Tallec, P. Richemond, E. Buchatskaya, C. Doersch, B. Avila Pires, Z. Guo, M. Gheshlaghi Azar *et al.*, "Bootstrap your own latent—a new approach to self-supervised learning," in *Advanced in Neural Information Processing Systems (NeurIPS)*, 2020.
- [28] A. Strehl and J. Ghosh, "Cluster ensembles—a knowledge reuse framework for combining multiple partitions," *Journal of Machine Learning Research*, vol. 3, no. 12, pp. 583–617, 2002.
- [29] D. Huang, C.-D. Wang, J.-S. Wu, J.-H. Lai, and C.-K. Kwok, "Ultra-scalable spectral clustering and ensemble clustering," *IEEE Transactions on Knowledge and Data Engineering*, vol. 32, no. 6, pp. 1212–1226, 2020.
- [30] D. Huang, C.-D. Wang, J.-H. Lai, and C.-K. Kwok, "Toward multidiversified ensemble clustering of high-dimensional data: From subspaces to metrics and beyond," *IEEE Transactions on Cybernetics*, pp. 1–14, 2021.
- [31] J. MacQueen *et al.*, "Some methods for classification and analysis of multivariate observations," in *Proc. of Mathematical Statistics and Probability*, 1967.
- [32] L. Zelnik-Manor and P. Perona, "Self-tuning spectral clustering," in *Advanced in Neural Information Processing Systems (NeurIPS)*, 2005.
- [33] K. C. Gowda and G. Krishna, "Agglomerative clustering using the concept of mutual nearest neighbourhood," *Pattern Recognition*, vol. 10, no. 2, pp. 105–112, 1978.
- [34] D. Cai, X. He, X. Wang, H. Bao, and J. Han, "Locality preserving non-negative matrix factorization," in *Proc. of International Joint Conference on Artificial Intelligence (IJCAI)*, 2009.
- [35] A. Martinez and A. Kak, "Pca versus lda," *IEEE Transactions on Pattern Analysis and Machine Intelligence*, vol. 23, no. 2, pp. 228–233, 2001.
- [36] T. Zhang, R. Ramakrishnan, and M. Livny, "BIRCH: An efficient data clustering method for very large databases," in *Proc. of SIGMOD International Conference on Management of Data*, 1996.
- [37] C. Fraley and A. E. Raftery, "Enhanced model-based clustering, density estimation, and discriminant analysis software: MCLUST," *Journal of Classification*, vol. 20, no. 2, pp. 263–286, 2003.
- [38] J. Xie, R. Girshick, and A. Farhadi, "Unsupervised deep embedding for clustering analysis," in *Proc. of International Conference on Machine Learning (ICML)*, 2016.
- [39] X. Guo, L. Gao, X. Liu, and J. Yin, "Improved deep embedded clustering with local structure preservation," in *Proc. of International Joint Conference on Artificial Intelligence (IJCAI)*, 2017.
- [40] X. Guo, X. Liu, E. Zhu, X. Zhu, M. Li, X. Xu, and J. Yin, "Adaptive self-paced deep clustering with data augmentation," *IEEE Transactions on Knowledge and Data Engineering*, vol. 32, no. 9, pp. 1680–1693, 2019.
- [41] Y. Tao, K. Takagi, and K. Nakata, "Clustering-friendly representation learning via instance discrimination and feature decorrelation," *arXiv preprint arXiv:2106.00131*, 2021.
- [42] L. Van der Maaten and G. Hinton, "Visualizing data using t-sne," *Journal of machine learning research*, vol. 9, no. 11, 2008.